

Heat transport by turbulent Rayleigh-Bénard convection for $\text{Pr} \simeq 0.8$ and $4 \times 10^{11} \lesssim \text{Ra} \lesssim 2 \times 10^{14}$: Ultimate-state transition for aspect ratio $\Gamma = 1.00$

Xiaozhou He^{1,6}, Denis Funfschilling^{2,6}, Eberhard Bodenschatz^{1,3,4,6}, and Guenter Ahlers^{5,6}

¹Max Planck Institute for Dynamics and Self-Organization (MPIDS), 37077 Göttingen, Germany

²LSGC CNRS - GROUPE ENSIC, BP 451, 54001 Nancy Cedex, France

³Institute for Nonlinear Dynamics, University of Göttingen, 37077 Göttingen, Germany

⁴Laboratory of Atomic and Solid-State Physics and Sibley School of Mechanical and Aerospace Engineering, Cornell University, Ithaca, NY 14853, USA

⁵Department of Physics, University of California, Santa Barbara, CA 93106, USA

⁶International Collaboration for Turbulence Research

Abstract. We report experimental results for heat-transport measurements, in the form of the Nusselt number Nu , by turbulent Rayleigh-Bénard convection in a cylindrical sample of aspect ratio $\Gamma \equiv D/L = 1.00$ ($D = 1.12$ m is the diameter and $L = 1.12$ m the height) and compare them with previously reported results for $\Gamma = 0.50$. The measurements were made using sulfur hexafluoride at pressures up to 19 bars as the fluid. They are for the Rayleigh-number range $4 \times 10^{11} \lesssim \text{Ra} \lesssim 2 \times 10^{14}$ and for Prandtl numbers Pr between 0.79 and 0.86.

For $\text{Ra} < \text{Ra}_1^* \simeq 2 \times 10^{13}$ we find $\text{Nu} = N_0 \text{Ra}^{\gamma_{eff}}$ with $\gamma_{eff} = 0.321 \pm 0.002$ and $N_0 = 0.0776$, consistent with classical turbulent Rayleigh-Bénard convection in a system with laminar boundary layers below the top and above the bottom plate and with the prediction of Grossmann and Lohse.

For $\text{Ra} > \text{Ra}_1^*$ the data rise above the classical-state power-law and show greater scatter. In analogy to similar behavior observed for $\Gamma = 0.50$, we interpret this observation as the onset of the transition to the ultimate state. Within our resolution this onset occurs at nearly the same value of Ra_1^* as it does for $\Gamma = 0.50$. This differs from an earlier estimate by Roche *et al.* which yielded a transition at $\text{Ra}_U \simeq 1.3 \times 10^{11} \Gamma^{-2.5 \pm 0.5}$. A Γ -independent Ra_1^* would suggest that the boundary-layer shear transition is induced by fluctuations on a scale less than the sample dimensions rather than by a global Γ -dependent flow mode. Within the resolution of the measurements the heat transport above Ra_1^* is equal for the two Γ values, suggesting a universal aspect of the ultimate-state transition and properties. The enhanced scatter of Nu in the transition region, which exceeds the experimental resolution, indicates an intrinsic irreproducibility of the state of the system.

Several previous measurements for $\Gamma = 1.00$ are re-examined and compared with the present results. None of them identified the ultimate-state transition.

1. Introduction

In this paper we consider turbulent convection in a fluid contained between horizontal parallel plates and heated from below (Rayleigh-Bénard convection or RBC; for reviews written for broad audiences see Refs. [1, 2]; for more specialized reviews see Refs. [3, 4]). It is now well established experimentally that RBC for Rayleigh numbers Ra (a dimensionless measure of the applied temperature difference ΔT) below a typical value Ra_1^* is a system with laminar (albeit fluctuating) boundary layers [5, 6] (BLs), one below the top and another above the bottom plate. Approximately half of $\Delta T \equiv T_b - T_t$ (T_b and T_t are the temperatures of the bottom and top confining plate respectively) is sustained by each of these BLs [7, 8, 9, 10, 11, 12, 13, 14]). The sample interior, known as the “bulk”, is nearly isothermal in the time average (see, however, Ref. [7, 15, 16, 17]), but its temperature and velocity fields are also fluctuating vigorously. This state is known as the “classical” state as it has been studied at great length for nearly a century.

At very large Ra a transition was predicted to take place [18, 19, 20] from the classical state to the “ultimate” state [21] where the BLs have become turbulent as well because of the shear applied to them by the vigorous fluctuations in the sample interior. Experimentally it was found recently for a cylindrical sample with aspect ratio $\Gamma \equiv D/L = 0.50$ (D is the diameter and L the height of the cylindrical sample) and $Pr \simeq 0.8$ that this transition takes place over a wide range $Ra_1^* \lesssim Ra \lesssim Ra_2^*$, with $Ra_1^* \simeq 1.5 \times 10^{13}$ and $Ra_2^* \simeq 5 \times 10^{14}$. For a more detailed description of the classical and ultimate state and the transition between them, see for instance Ref. [22] and the review articles [1, 2, 3].

The purpose of the present work was two-fold. First we hoped to determine with high accuracy the dependence of Nu on Ra in the classical state at the largest-possible Rayleigh numbers for a sample of aspect ratio $\Gamma = 1.00$ and for a Prandtl number $Pr \simeq 0.8$. Such data make it possible to test in detail the predictions for the classical state by Grossmann and Lohse [23, 24] of the relationship between Nu and Ra in a parameter range not explored heretofore. Although in principle these predictions should be applicable to the classical state regardless of Γ , they depend on a number of parameters that had been determined by fitting to experimental data for $\Gamma = 1.00$ [25]. This fit was done over the range $4 \lesssim Pr \lesssim 34$ and $3 \times 10^7 \lesssim Ra \lesssim 3 \times 10^9$. Thus, a comparison with new data over the very different Ra and Pr ranges of the present work constitutes a significant test of the prediction. We found that $Nu = N_0 Ra^{\gamma_{eff}}$ with $N_0 = 0.0776$ and $\gamma_{eff} = 0.321 \pm 0.002$. This result differs slightly from the case $\Gamma = 0.50$ [22] which yielded $\gamma_{eff} = 0.312 \pm 0.002$. It is in excellent agreement with the Grossmann-Lohse prediction for the classical state and $\Gamma = 1.00$ in our Ra and Pr range.

Second, we hoped to search for the transition to the “ultimate” state of turbulent convection. Experiments searching for this state using $\Gamma = 0.50$ had been carried out before [26, 27, 21, 28, 29, 30, 31, 32, 33, 34, 35]; results from these searches were reported and/or reviewed in another publication [22]. The transition was found very recently

[36, 22] to occur over a wide Ra-range, extending from $Ra_1^* \simeq 2 \times 10^{13}$ to $Ra_2^* \simeq 5 \times 10^{14}$. In the present project we focus on the particular case of a cylindrical sample with $\Gamma = 1.00$ ($D = 1.12$ m and $L = 1.12$ m). This geometry was used in some previous searches for this state [37, 38, 39, 35, 40] and thus enables a direct comparison with earlier measurements; but more importantly we chose $\Gamma = 1.00$ in order to search for any Γ -dependence of the transition. Earlier a transition in $Nu(Ra)$ had been reported at several Γ values by Roche *et al.* [35] at Rayleigh numbers $Ra_U \simeq 1.3 \times 10^{11} \Gamma^{-2.5 \pm 0.5}$ which those authors attributed to the ultimate-state transition. In contradistinction to this result, we find that the transition occurs at values of Ra that are two orders of magnitude larger than Ra_U , and that (for $\Gamma = 0.50$ and 1.00) Ra_1^* is independent of Γ within the resolution of the data. A Γ -independent Ra_1^* would suggest that the boundary-layer shear-transition is induced by fluctuations on a scale less than the sample dimensions rather than by a global Γ -dependent flow mode. Within the resolution of the results the heat transport above Ra_1^* is equal for the two Γ values, suggesting a universal aspect of the ultimate-state transition and properties. Unfortunately the necessarily smaller height of the $\Gamma = 1.00$ sample (compared to $\Gamma = 0.50$) limited our measurement range to $Ra \lesssim 2 \times 10^{14}$ and prevented us from obtaining data all the way beyond Ra_2^* .

Our results were obtained using the High-Pressure Convection Facility (the HPCF, a cylindrical sample of 1.12 m diameter) at the Max Planck Institute for Dynamics and Self-organization in Göttingen, Germany with sulfur hexafluoride (SF_6) at pressures up to 19 bars as the fluid. Results for $\Gamma = 0.50$ from this work were presented in Refs. [41, 42, 43, 36, 22]. A description of the apparatus was given in Ref. [41]. The present paper presents new results obtained for a sample chamber known as HPCF-IV which had a height equal to its diameter.

In Sec. 2 we define the parameters that describe this system. Then, in Sec. 3, we give a brief discussion of the apparatus used in this work. A detailed description of the main features was presented before [41]. Section 4 presents a comprehensive discussion of our results and of the results of others at large Ra for cylindrical samples with $\Gamma = 1.00$. We conclude with a Summary in Sec. 5.

2. The system parameters and data analysis.

For turbulent RBC in cylindrical containers there are two parameters which, in addition to Γ , are expected to determine its state. They are the dimensionless temperature difference as expressed by the Rayleigh number

$$Ra \equiv \frac{\alpha g \Delta T L^3}{\kappa \nu} \quad (1)$$

and the ratio of viscous to thermal dissipation as given by the Prandtl number

$$Pr \equiv \nu / \kappa . \quad (2)$$

Here α is the isobaric thermal expansion coefficient, g the gravitational acceleration, κ the thermal diffusivity, ν the kinematic viscosity, and $\Delta T \equiv T_b - T_t$ the applied temperature difference between the bottom (T_b) and the top (T_t) plate.

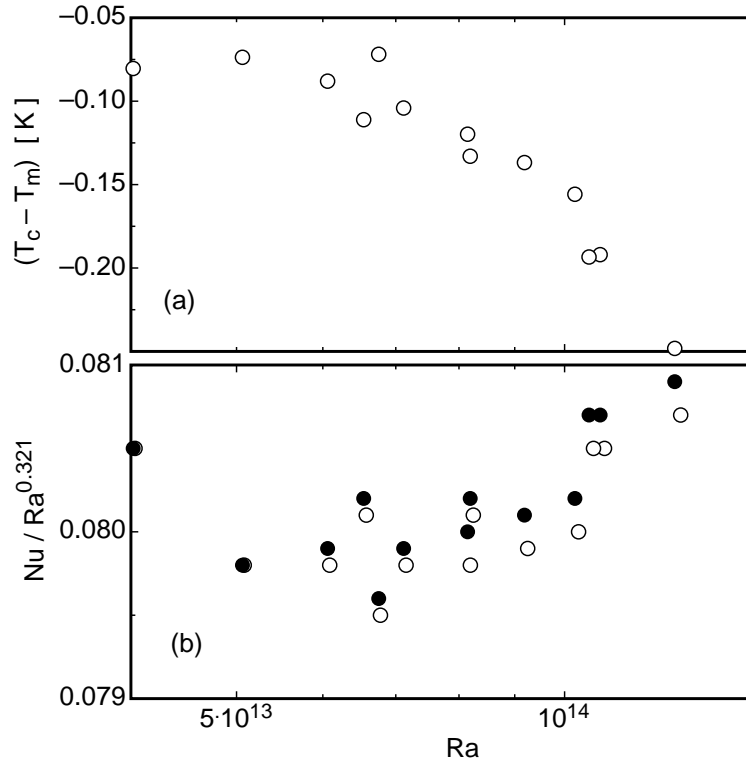


Figure 1. (a): The difference between the center temperature T_c and the mean temperature T_m of the sample as a function of Ra . The sample pressure was 18.6 bars. (b): The reduced Nusselt number $Nu/Ra^{0.321}$ as a function of the Rayleigh number Ra . Solid circles: all fluid properties evaluated at T_m . Open circles: All fluid properties evaluated at T_c .

In the present paper we present measurements of the heat transport in the form of the scaled effective thermal conductivity known as the Nusselt number, which is given by

$$Nu \equiv \frac{QL}{A\Delta T\lambda}. \quad (3)$$

Here Q is the applied heat current, $A = D^2\pi/4$ the sample cross-sectional area, and λ the thermal conductivity. The measurements cover the range $5 \times 10^{11} \lesssim Ra \lesssim 2 \times 10^{14}$ and are for Pr ranging from 0.79 at the lowest to 0.86 at the highest Ra .

All fluid properties needed to calculate Ra , Pr , and Nu were evaluated at the mean temperature $T_m = (T_t + T_b)/2$ of the sample. They were obtained from numerous papers in the literature, as discussed in Ref. [44]. A small correction for the nonlinear contribution of the side-wall conductance [45, 46] to the heat carried by the sample was no more than 3% and was applied to the data.

In a recent communication [47] it was suggested that the fluid properties should be evaluated at the sample center temperature T_c rather than at T_m in order to avoid or minimize effects due to departures from the Oberbeck-Boussinesq (OB) approximation [48, 49]. We note that this would be contrary to the convention adopted in the usual studies of non-OB effects (see, for instance, [50, 51, 52]). Nonetheless we explored the

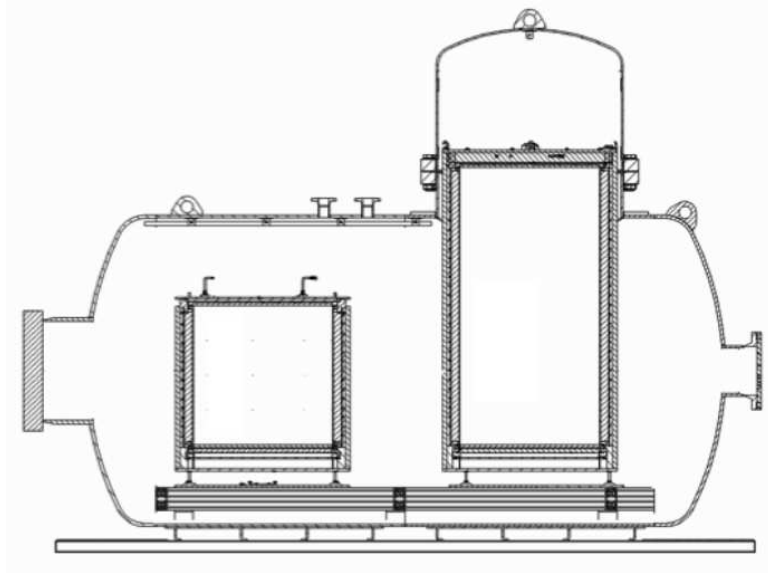


Figure 2. A schematic diagram, to scale, of the Uboot with HPCF-II (right) and HPCF-IV (left).

importance of the choice between T_c and T_m for our data. In Fig. 1a we show $T_c - T_m$ as a function of Ra at the largest Ra of our work where its magnitude is also largest. In Fig. 1b we show the corresponding reduced Nusselt numbers $Nu/Ra^{0.321}$ as a function of Ra . The solid (open) circles are based on fluid properties evaluated at T_m (T_c). One sees that the largest difference, which occurs at the largest Ra , is only about a third of a percent. Such a difference is essentially negligible and does not influence the interpretation of our results.

The data obtained in this study are presented as an Appendix to this paper.

3. Apparatus

The apparatus was the same as the one described before [41], except that a new sample cell, known as the High-Pressure Convection-Facility IV or HPCF-IV, was constructed. This cell had an internal height $L = 1120 \pm 2$ mm and a diameter D equal to L , yielding an aspect ratio $\Gamma \equiv D/L = 1.000 \pm 0.004$. It had the aluminum top and bottom plates described in Ref. [41], and a 9.5 mm thick plexiglas side wall. The plates were sealed to the side wall, and a tube of 13 mm diameter entered the HPCF-IV at mid height through the side wall to permit filling the sample cell with gas to the desired pressure. This tube was sealed by a remotely controlled valve after the sample was filled and all transients had decayed, yielding a completely closed sample. All thermal shields were duplicates of those used for another sample with $\Gamma = 0.50$ known as HPCF-II [53], except that the side shield was of course shorter. The HPCF-IV was located in a high-pressure vessel known as the Uboot of Göttingen which could be filled with sulfur hexafluoride (SF_6) at pressures up to 19 bars. The Uboot could contain HPCF-IV and as well as HPCF-II simultaneously, as shown in the schematic

diagram Fig. 2. Completely separate instrumentation and temperature-controlled water circuits enabled simultaneous measurements in the two units. We refer to our previous publications [41, 22] for detailed descriptions of all construction details and experimental procedures.

4. Results

4.1. Classical state

In Fig. 3a we show results for Nu as a function of Ra on double logarithmic scales. The data for $\Gamma = 1.00$ are shown in black, and previously published results [36, 22] for $\Gamma = 0.50$ (HPCF-II) are given in red. One sees that, within the resolution of this graph, there is very little difference between the data for the two Γ values. Also shown in this figure, as a vertical dotted line, is the approximate upper limit of the classical regime and the beginning of the transition range to the ultimate state at $Ra_1^* = 1.5 \times 10^{13}$ as determined from the $\Gamma = 0.50$ data and reported in Ref. [36].

The solid black and dash-dotted red lines are fits of the power law

$$Nu = N_0 Ra^{\gamma_{eff}} \quad (4)$$

to the data with $Ra < Ra_1^*$. As reported elsewhere [22], the fit to the $\Gamma = 0.50$ data yielded $\gamma_{eff} = 0.312 \pm 0.002$. The fit to the $\Gamma = 1.00$ data for $Ra < Ra_1^*$ gave $N_0 = 0.0764 \pm 0.0015$ and $\gamma_{eff} = 0.3216 \pm 0.0007$ where the uncertainties are the standard errors of the parameters. The average value of Pr over the range of the data used in the fit was 0.80. Additional possible systematic errors, primarily due to uncertainties in the side-wall correction, lead us to the best estimate $\gamma_{eff} = 0.321 \pm 0.002$ for the Nusselt exponent for $\Gamma = 1.00$ and $Pr = 0.80$. Fixing γ_{eff} at the value 0.321 led to the amplitude $N_0 = 0.0776$.

In order to provide a better comparison of these two data sets, we show the results in the form of the reduced Nusselt number $Nu/Ra^{0.321}$ as a function of Ra on double logarithmic scales in Fig. 3b. Now the $\Gamma = 1.00$ data scatter about the horizontal solid black line, with the scatter corresponding to a standard deviation of 0.21%.

In Fig. 3b the power-law fit to the $\Gamma = 0.50$ data is shown again as a red dash-dotted line. One can readily see the positive deviations and enhanced scatter of the $\Gamma = 0.50$ data for $Ra > Ra_1^*$ where the transition to the ultimate state is beginning. We note that the enhanced scatter is not due to a sudden increase in experimental scatter, but rather a reflection of the intrinsic irreproducibility of the state of the system. Remarkably, also the $\Gamma = 1.00$ data begin to show positive deviations from the horizontal black line and enhanced scatter, suggesting that also the $\Gamma = 1.00$ system is undergoing a similar transition to the ultimate state, beginning at about the same Ra_1^* that was found for $\Gamma = 0.50$. We shall return to that issue below in Sec. 4.3.

We also show in Fig. 3b, as a short-dashed blue line, the prediction of Grossmann and Lohse [24] (GL) for $Nu(Ra)$ in the classical state with $Pr = 0.80$. This prediction is based on two coupled equations with several parameters which had been determined

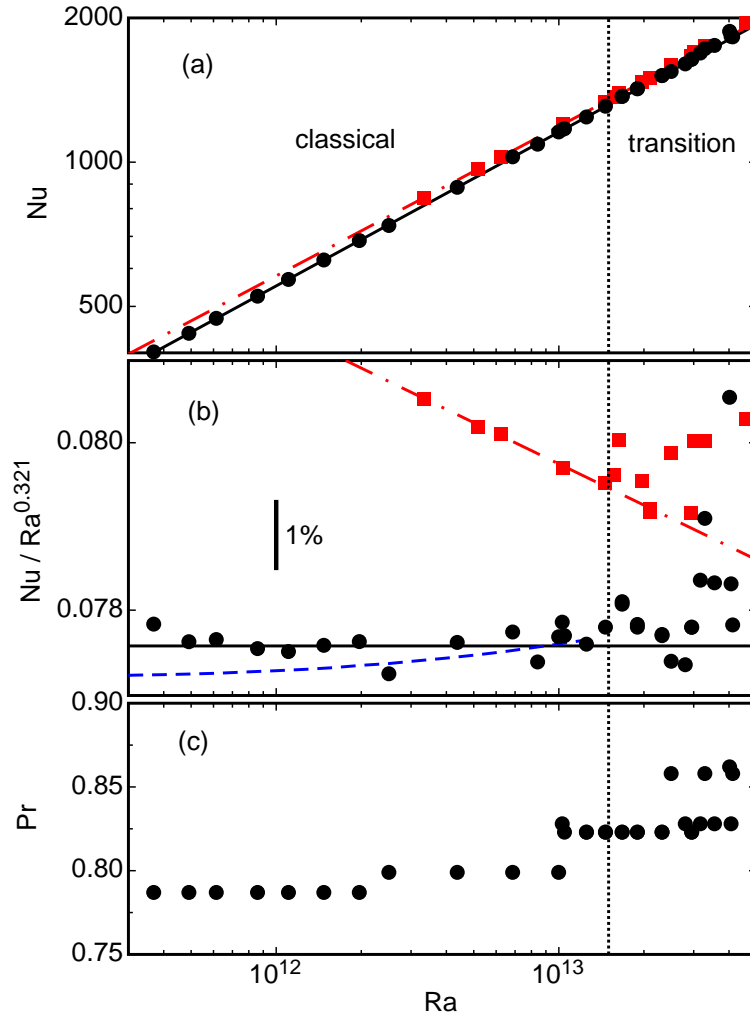


Figure 3. (a): The Nusselt number Nu as a function of the Rayleigh number Ra on logarithmic scales. Black circles: $\Gamma = 1.00$ (HPCF-IV, current work). Red squares: $\Gamma = 0.50$ (HPCF-IIe, Refs. [36, 22]). The solid black line is a power-law fit to the data for $\Gamma = 1.00$ in the classical state $Ra < 1.5 \times 10^{13}$. The fit gave $N_0 = 0.0764 \pm 0.0015$ and $\gamma_{eff} = 0.3216 \pm 0.0007$. The red dash-dotted line is the power-law fit to the data in the classical state for $\Gamma = 0.50$ which gave $N_0 = 0.1404$, $\gamma_{eff} = 0.312$, see Ref. [36, 22]. The vertical dotted line is the location of Ra_1^* as determined for $\Gamma = 0.50$ [36, 22]. (b): The reduced Nusselt number $Nu/Ra^{0.321}$ as a function of Ra on logarithmic scales. All symbols and lines are as in (a). We added the blue short-dashed line, which is the prediction of Grossmann and Lohse [24]. (c): The Prandtl numbers as a function of Ra for all data points within the range of this figure.

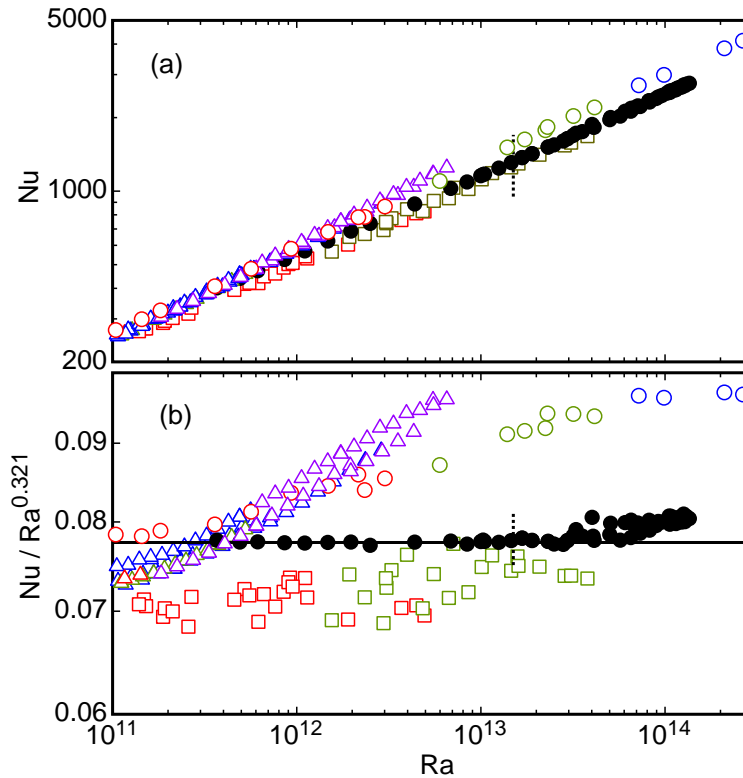


Figure 4. Comparison of our results (black solid circles, $0.79 \leq Pr \leq 0.86$) with the data of previous investigations. For the previous work we show data with $Pr < 1$ in red, data with $1 < Pr < 2$ in green, data with $2 < Pr < 4$ in blue, and data with $Pr > 4$ in purple. Open circles: Niemela and Sreenivasan [38]. Open up-pointing triangles: Roche *et al.* [35]. Open squares: Urban *et al.* [40]. The short vertical dotted line represents $Ra_1^* = 1.5 \times 10^{13}$ as determined for $\Gamma = 0.50$ [36, 22].

by fits to experimental data [25] for $\Gamma = 1.00$ over the parameter ranges $4 \lesssim Pr \lesssim 34$ and $3 \times 10^7 \lesssim Ra \lesssim 2 \times 10^9$. One sees that the comparison with the present data up to $Ra = 10^{13}$ and for $Pr \simeq 0.80$ requires a considerable extrapolation. Thus, the excellent agreement is indeed remarkable. Not only does it require a high degree of reliability of the GL equations; it also requires excellent consistency between the experimental data used to determine the free parameters in these equations and the present data.

4.2. Comparison with published data

In Fig. 4 we compare our results with other published data for $\Gamma = 1.00$ (a detailed comparison with literature data for $\Gamma = 0.50$ is being presented elsewhere [22]). Here too we show Nu in Fig. 4a and, for higher resolution, $Nu/Ra^{0.321}$ in Fig. 4b. For the literature data we use red symbols for data with $Pr < 1$, green symbols for data with $1 < Pr < 2$, blue symbols for data with $2 < Pr < 4$, and purple symbols for data with $Pr > 4$. Our own data span the range from $Pr = 0.79$ at the lowest to $Pr = 0.86$ at the highest Ra .

The present results are given as solid black circles. The data of Niemela and

Sreenivasan [38] are shown as open circles. For Ra near 10^{11} they follow a power law with an exponent near 0.33; but for $3 \times 10^{11} \lesssim Ra \lesssim 5 \times 10^{13}$ they rise more steeply, only to level off again for larger Ra to a dependence describable once more by an effective exponent near 0.33. This behavior was attributed by the authors [54] to a special type of non-Boussinesq effect near critical points. Thus the data do not yield reliable parameters of a power law for $Nu(Ra)$ in the classical region that could be compared with the prediction of GL [24]; according to the authors [54] the data also do not yield any evidence for a transition to the ultimate state.

The data for the “short cell” of Roche *et al.* are shown as open up-pointing triangles. They reveal a gradual increase of an effective exponent, starting near $Ra = 5 \times 10^{10}$. Although the authors believe that this rise of the exponent is indicative of an ultimate-state transition at $Ra_U \simeq 10^{11}$, we do not find the evidence convincing. Particularly troublesome is the low value of Ra_U ; it is unlikely that the boundary-layer shear Reynolds-number Re_s can be high enough to drive the BLs turbulent at so low a value of Ra [36]. Very recent direct numerical simulations (DNS) for $\Gamma = 1$ and $Pr = 0.7$ [55] suggest that $Re_s \simeq 65$ for $Ra = 10^{11}$, a value much too low to expect a shear instability to turbulence (for the higher Pr values of the experiment Re_s would be even lower). On the other hand, we do not have an alternative explanation of the rise of γ_{eff} indicated by these data.

A third set of data (open squares in Fig. 4) was published recently by Urban *et al.* [40]. They extend up to $Ra \simeq 4 \times 10^{13}$. Although at constant $Pr \simeq 0.8$ one might have hoped to have reached Ra_1^* at that point, Pr also rose significantly at these large Ra , and one expects that Ra^* increases significantly with Pr . In any event, no indication of an ultimate-state transition is seen in these data, nor is one claimed by their authors.

In view of the above it is our view that the ultimate-state transition has not yet been seen in any of the published data for $\Gamma \simeq 1$.

4.3. Transition toward the ultimate state

Recent measurements [36] for a $\Gamma = 0.50$ sample revealed that the transition to the ultimate state for that aspect ratio occurred over the approximate range from $Ra_1^* = 1.5 \times 10^{13}$ to $Ra_2^* = 5 \times 10^{14}$. We show those data in Fig. 5 as open circles and compare them with our new data for $\Gamma = 1.00$ (solid circles). The vertical dotted lines in the figure indicate the locations of Ra_1^* and Ra_2^* . In the classical range below Ra_1^* both data sets follow a power law, albeit with the slightly different exponents of 0.312 for $\Gamma = 0.50$ and 0.321 for $\Gamma = 1.00$. Near Ra_1^* *both* data sets rise above their respective classical-state power laws, and the enhanced scatter of both data sets reveals the intrinsic irreproducibility of the state of the system in the Ra range of the transition from the classical to the ultimate state. Although in the classical state the two systems had slightly different Nusselt numbers, it is remarkable that in the transition region they display the same Nu values within the resolution allowed by the intrinsic scatter of the two systems. Unfortunately, in view of the smaller height of the $\Gamma = 1.00$ sample, our

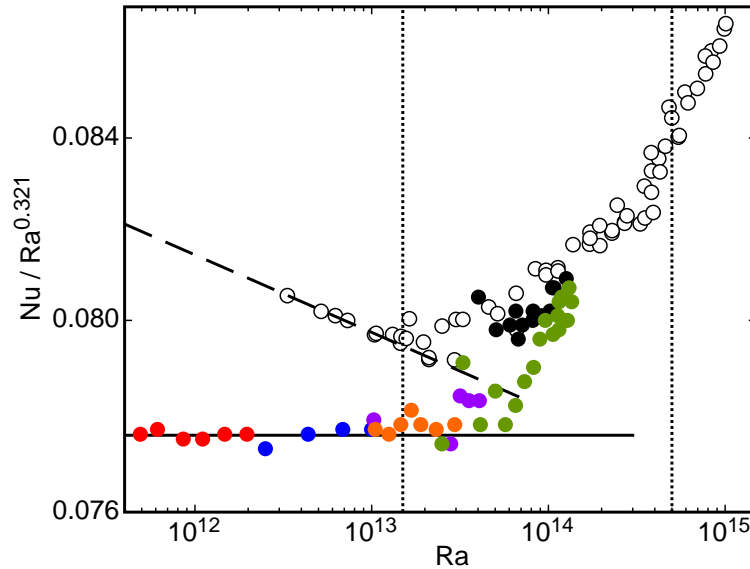


Figure 5. High-resolution comparison of the results for $\Gamma = 0.50$ (HPCF-IIe, Ref. [36, 22], open symbols) with the present results for $\Gamma = 1.00$ (HPCF-IV, solid circles). For $\Gamma = 1.00$ the data were taken at pressures of 4.1 bars (red, $Pr = 0.79$), 7.9 bars (blue, $Pr = 0.80$), 12.1 bars (orange, $Pr = 0.82$), 12.9 bars (purple, $Pr = 0.83$), 17.7 bars (green, $Pr = 0.86$), and 18.6 bars (black, $Pr = 0.86$). The vertical dotted lines are the locations $Ra_1^* = 1.5 \times 10^{13}$ and $Ra_2^* = 5 \times 10^{14}$ as determined for $\Gamma = 0.50$. The dashed line is a power-law fit to the data in the classical state for $\Gamma = 0.50$ and corresponds to $N_0 = 0.1044$ and $\gamma_{eff} = 0.312$. The solid line is a power-law fit to the data in the classical state for $\Gamma = 1.00$ (HPCF-IV) which gave $N_0 = 0.0776$ and $\gamma_{eff} = 0.321$.

measurements are limited to $Ra \lesssim 2 \times 10^{14}$. Thus it is not possible for us to follow the transition all the way beyond Ra_2^* , as was done for $\Gamma = 0.50$ with HPCF-II.

Finally we note that an extrapolation of the shear Reynolds numbers obtained from DNS [55] for $\Gamma = 1.00$ and $Pr = 0.7$ yields $Re_s \simeq 250$ for $Ra = Ra_1^* = 1.5 \times 10^{13}$. This is a reasonable value for the onset of the boundary-layer shear transition to the ultimate state. It is also similar to the value of $Re_s(Ra_1^*)$ deduced from experimental determinations of Re for $\Gamma = 0.50$ [36].

5. Summary

In this paper we presented new data for heat transport, expressed as the Nusselt number Nu , by turbulent Rayleigh-Bénard convection in a cylindrical sample of aspect ratio $\Gamma = 1.00$ over the Ra range $4 \times 10^{11} \lesssim Ra \lesssim 2 \times 10^{14}$. We note that the Prandtl number was nearly constant for our work, varying only from about 0.79 at our smallest to about 0.86 at our largest Ra . This stands in contrast to other measurements [38, 35, 40] which were made near the critical point of helium, where Pr typically varied from about 0.7 to about 4 over the same Ra range. Maintaining a constant Pr is important in the search for the ultimate-state transition because the transition range is expected to shift

to larger Ra as Pr increases, approximately in proportion to $Pr^{1.6}$ [56].

In the classical regime for Rayleigh numbers $Ra \lesssim Ra_1^* = 1.5 \times 10^{13}$ we found that our measurements are in remarkably good agreement with the predictions of Grossmann and Lohse [24] (GL). We note that this agreement not only implies excellent reliability of the prediction. It also indicates consistency of the new data for $Pr \simeq 0.8$ and $5 \times 10^{11} \lesssim Ra \lesssim 1.5 \times 10^{13}$ with measurements [25] made a decade ago, using very different experimental techniques and organic fluids rather than compressed gases, since these older data for $4 \lesssim Pr \lesssim 34$ and $3 \times 10^7 \lesssim Ra \lesssim 2 \times 10^9$ were used to fix the free parameters of the equations derived by GL.

We compared the $\Gamma = 1.00$ results with previous measurements for $\Gamma = 0.50$. In the classical regime we found that the two geometries yielded slightly different effective exponents of the power laws that describe $Nu(Ra)$. For $\Gamma = 0.50$ we reported elsewhere [22] that $\gamma_{eff} = 0.312 \pm 0.002$. For $\Gamma = 1.00$ we now find that $\gamma_{eff} = 0.321 \pm 0.002$, in excellent agreement with the GL result $\gamma_{eff} = 0.323$ in our parameter range.

In the classical range $Ra \lesssim Ra_1^* = 1.5 \times 10^{13}$ the data had very little scatter, with root-mean-square deviations from the power-law fit as small as 0.2%. At larger Ra the scatter increased, indicating an intrinsic irreproducibility of the state of the system from one data point to another. Further, most of the points for $Ra > Ra_1^*$ fell well above the power-law extrapolation from the classical state. Both of these phenomena were seen as well at the beginning of the transition to the ultimate state for $\Gamma = 0.5$ [36]. Indeed, for $Ra > Ra_1^*$ the $\Gamma = 1.00$ data agree quite closely with the $\Gamma = 0.50$ data. Thus we believe that we observed the onset of the transition to the ultimate state also for $\Gamma = 1.00$, and that Ra_1^* for $\Gamma = 1.00$ is very nearly the same as it is for $\Gamma = 0.50$. Earlier measurements by Roche *et al.* [35] had revealed a transition in $Nu(Ra)$ at several Γ values at Rayleigh numbers $Ra_U \simeq 1.3 \times 10^{11} \Gamma^{-2.5 \pm 0.5}$ which those authors attributed to the ultimate-state transition (for a detailed discussion of some of those data, see Ref. [22]). In contradistinction to this result, the transitions found by us for $\Gamma = 0.50$ and 1.00 are, within the resolution of the data, independent of Γ . We believe that a Γ -independent Ra_1^* suggests that the boundary-layer shear-transition is induced by fluctuations on a scale less than the sample dimensions rather than by a global Γ -dependent flow mode. Above Ra_1^* any difference between the heat transport for the two Γ values is too small to be resolved, suggesting a universal aspect of the ultimate-state transition and properties. Unfortunately the smaller height of the $\Gamma = 1.00$ sample, compared to $\Gamma = 0.50$, limits the accessible range to $Ra \lesssim 2 \times 10^{14}$. Thus, for this case, we were able to cover only a little more than the lower half of the transition range to the ultimate state.

Acknowledgments

We are very grateful to the Max-Planck-Society and the Volkswagen Stiftung, whose generous support made the establishment of the facility and the experiments possible. We thank the Deutsche Forschungsgemeinschaft (DFG) for financial support through

SFB963: “Astrophysical Flow Instabilities and Turbulence”. The work of G.A. was supported in part by the U.S National Science Foundation through Grant DMR11-58514. We thank Andreas Kopp, Artur Kubitzeck, and Andreas Renner for their enthusiastic technical support. We are very grateful to Holger Nobach for many useful discussions and for his contributions to the assembly of the experiment.

Appendix A. Data tables.**Table A1.** SF₆, HPCF-IV. The data are presented in chronological order.

Run No.	P (bars)	T_m (°C)	ΔT (K)	Ra	Pr	Nu
120227	18.557	21.067	6.534	6.752e+13	0.862	2189.32
120228	18.540	21.309	10.603	1.078e+14	0.862	2577.65
120229	18.537	21.551	10.492	1.053e+14	0.862	2559.41
120301	18.571	21.536	12.461	1.262e+14	0.862	2720.43
120302	18.581	21.599	8.091	8.192e+13	0.862	2346.32
120303	18.555	21.546	6.486	6.541e+13	0.862	2183.10
120304	18.530	21.557	4.012	4.019e+13	0.862	1874.97
120307	18.559	21.503	5.005	5.063e+13	0.862	2001.59
120308	18.566	21.491	5.978	6.061e+13	0.862	2122.51
120309	18.574	21.508	7.011	7.117e+13	0.862	2233.55
120310	18.583	21.506	8.007	8.147e+13	0.862	2335.39
120311	18.592	21.509	9.011	9.187e+13	0.862	2429.87
120312	18.600	21.502	9.996	1.022e+14	0.862	2517.33
120314	4.058	21.508	4.020	4.910e+11	0.787	439.40
120315	4.068	21.517	16.029	1.968e+12	0.787	686.14
120316	4.064	21.518	12.035	1.474e+12	0.787	624.99
120317	4.061	21.516	9.032	1.105e+12	0.787	569.24
120318	4.060	21.513	7.027	8.589e+11	0.787	525.25
120319	4.058	21.513	5.026	6.137e+11	0.787	472.17
120320	4.057	21.511	3.021	3.686e+11	0.787	401.83
120322	7.953	21.499	15.992	9.984e+12	0.799	1156.44
120323	7.944	21.511	11.030	6.863e+12	0.799	1026.08
120324	7.940	21.518	7.033	4.370e+12	0.799	886.28
120325	7.934	21.520	4.038	2.504e+12	0.799	737.70
120329	12.919	21.515	4.027	1.028e+13	0.828	1169.92
120331	12.894	21.524	11.043	2.801e+13	0.828	1603.61
120401	12.913	21.475	15.941	4.068e+13	0.828	1829.93
120402	12.903	21.485	13.963	3.554e+13	0.828	1752.55
120403	12.898	21.485	12.464	3.167e+13	0.828	1689.55
120404	17.649	21.409	11.808	9.604e+13	0.858	2462.53
120405	17.612	21.357	16.199	1.309e+14	0.858	2742.66
120406	17.528	20.463	14.413	1.188e+14	0.857	2655.13
120407	17.533	20.472	13.931	1.149e+14	0.858	2623.51
120408	17.616	20.454	13.396	1.129e+14	0.858	2596.70
120409	17.689	21.454	16.534	1.355e+14	0.858	2764.66

120410	17.737	21.493	15.472	1.281e+14	0.859	2702.71
120411	17.727	21.411	14.807	1.227e+14	0.859	2663.98
120413	17.683	21.513	4.025	3.285e+13	0.858	1725.56
120415	17.763	21.439	9.869	8.241e+13	0.859	2316.20
120416	17.725	21.544	6.086	5.011e+13	0.859	1961.69
120417	17.741	21.392	13.774	1.147e+14	0.859	2601.23
120417	17.730	21.407	12.802	1.062e+14	0.859	2535.08
120418	17.710	21.429	10.850	8.949e+13	0.859	2394.85
120418	17.689	21.480	8.954	7.330e+13	0.858	2220.76
120419	17.678	21.502	6.999	5.709e+13	0.858	2028.18
120419	17.674	21.501	7.997	6.517e+13	0.858	2124.46
120420	17.679	21.531	5.057	4.121e+13	0.858	1826.17
120420	17.678	21.535	3.066	2.497e+13	0.858	1546.36
120423	12.173	21.497	13.987	2.951e+13	0.823	1639.95
120424	12.160	21.517	11.031	2.318e+13	0.823	1516.00
120425	12.149	21.527	9.052	1.896e+13	0.823	1423.45
120426	12.131	21.518	8.032	1.675e+13	0.823	1372.14
120427	12.097	21.539	7.077	1.462e+13	0.823	1308.59
120428	12.096	21.531	6.060	1.252e+13	0.823	1242.46
120829	12.088	21.542	5.082	1.047e+13	0.823	1174.20

- [1] L. P. Kadanoff, *Turbulent heat flow: Structures and scaling*, Phys. Today **54**, 34 (2001).
- [2] G. Ahlers, *Turbulent convection*, Physics **2**, 74 (2009).
- [3] G. Ahlers, S. Grossmann, and D. Lohse, *Heat transfer and large scale dynamics in turbulent Rayleigh-Bénard convection*, Rev. Mod. Phys. **81**, 503 (2009).
- [4] D. Lohse and K.-Q. Xia, *Small-scale properties of turbulent Rayleigh-Bénard convection*, Annu. Rev. Fluid Mech. **42**, 335 (2010).
- [5] Q. Zhou and K.-Q. Xia, *Measured Instantaneous Viscous Boundary Layer in Turbulent Rayleigh-Bénard Convection*, Phys. Rev. Lett. **104**, 104301 (4 pages) (2010).
- [6] R. J. A. M. Stevens, Q. Zhou, S. Grossmann, R. Verzicco, K.-Q. Xia, and D. Lohse, *Thermal boundary layer profiles in turbulent Rayleigh-Bénard convection in a cylindrical sample*, Phys. Rev. E **85**, 027301 (2012).
- [7] A. Tilgner, A. Belmonte, and A. Libchaber, *Temperature and velocity profiles of turbulence convection in water*, Phys. Rev. E **47**, R2253 (1993).
- [8] A. Belmonte, A. Tilgner, and A. Libchaber, *Boundary layer length scales in thermal turbulence*, Phys. Rev. Lett. **70**, 4067 (1993).
- [9] A. Belmonte, A. Tilgner, and A. Libchaber, *Temperature and velocity boundary layers in turbulent convection*, Phys. Rev. E **50**, 269 (1994).
- [10] Y. B. Xin and K.-Q. Xia, *Boundary layer length scales in convective turbulence*, Phys. Rev. E **56**, 3010 (1997).
- [11] S. L. Lui and K.-Q. Xia, *Spatial structure of the thermal boundary layer in turbulent convection*, Phys. Rev. E **57**, 5494 (1998).
- [12] S. Q. Zhou and K.-Q. Xia, *Scaling properties of the temperature field in convective turbulence*, Phys. Rev. Lett. **87**, 064501 (2001).
- [13] J. Wang and K.-Q. Xia, *Spatial variations of the mean and statistical quantities in the thermal boundary layers of turbulent convection*, Eur. Phys. J. B **32**, 127 (2004).
- [14] R. du Puits, C. Resagk, A. Tilgner, F. H. Busse, and A. Thess, *Structure of thermal boundary layers in turbulent Rayleigh-Bénard convection*, J. Fluid Mech. **572**, 231 (2007).
- [15] E. Brown and G. Ahlers, *Temperature gradients, and search for non-Boussinesq effects, in the interior of turbulent Rayleigh-Benard convection*, Europhys. Lett. **80**, 14001 (2007).
- [16] S. Weiss and G. Ahlers, *Turbulent Rayleigh-Bénard convection in a cylindrical container with aspect ration $\Gamma = 0.50$ and Prandtl number $Pr=4.38$* , J. Fluid Mech. **676**, 5 (2011).
- [17] G. Ahlers, E. Bodenschatz, D. Funfschilling, S. Grossmann, X. He, D. Lohse, R. Stevens, and R. Verzicco, *Logarithmic temperature profiles in turbulent Rayleigh-Bénard convection*, Phys. Rev. Lett., submitted, (2012) (arXiv:physics.flu-dyn/1204.6465).
- [18] R. H. Kraichnan, *Turbulent thermal convection at arbitrary Prandtl number*, Phys. Fluids **5**, 1374 (1962).
- [19] E. A. Spiegel, *Convection in stars*, Ann. Rev. Astron. Astrophys. **9**, 323 (1971).
- [20] S. Grossmann and D. Lohse, *Multiple scaling in the ultimate regime of thermal convection*, Phys. Fluids **23**, 045108 (2011).
- [21] X. Chavanne, F. Chilla, B. Castaing, B. Hebral, B. Chabaud, and J. Chaussy, *Observation of the ultimate regime in Rayleigh-Bénard convection*, Phys. Rev. Lett. **79**, 3648 (1997).
- [22] G. Ahlers, X. He, D. Funfschilling, and E. Bodenschatz, *Heat transport by turbulent Rayleigh-Bénard convection for $Pr \simeq 0.8$ and $Ra \lesssim 10^{15}$: Aspect ratio $\Gamma = 0.50$* , New J. Phys. submitted, (2012) (arXiv:physics.flu-dyn/1205.0108).
- [23] S. Grossmann and D. Lohse, *Scaling in thermal convection: A unifying view*, J. Fluid. Mech. **407**, 27 (2000).
- [24] S. Grossmann and D. Lohse, *Thermal convection for large Prandtl number*, Phys. Rev. Lett. **86**, 3316 (2001).
- [25] G. Ahlers and X. Xu, *Prandtl-number dependence of heat transport in turbulent Rayleigh-Bénard convection*, Phys. Rev. Lett. **86**, 3320 (2001).
- [26] B. Castaing, G. Gunaratne, F. Heslot, L. Kadanoff, A. Libchaber, S. Thomae, X. Z. Wu, S.

- Zaleski, and G. Zanetti, *Scaling of hard thermal turbulence in Rayleigh-Bénard convection*, J. Fluid Mech. **204**, 1 (1989).
- [27] X. Chavanne, F. Chillá, B. Chabaud, B. Castaing, J. Chaussey, and B. Hébral, *High Rayleigh number convection with gaseous helium at low temperature*, J. Low Temp. Phys. **104**, 109 (1996).
- [28] J. J. Niemela, L. Skrbek, K. R. Sreenivasan, and R. Donnelly, *Turbulent convection at very high Rayleigh numbers*, Nature **404**, 837 (2000).
- [29] J. J. Niemela, L. Skrbek, K. R. Sreenivasan, and R. Donnelly, *Turbulent convection at very high Rayleigh numbers*, Nature **406**, 439 (erratum) (2000).
- [30] X. Chavanne, F. Chilla, B. Chabaud, B. Castaing, and B. Hebral, *Turbulent Rayleigh-Bénard convection in gaseous and liquid He*, Phys. Fluids **13**, 1300 (2001).
- [31] P. E. Roche, B. Castaing, B. Chabaud, and B. Hebral, *Observation of the 1/2 power law in Rayleigh-Bénard convection*, Phys. Rev. E **63**, 045303 (2001).
- [32] P. Roche, F. Gauthier, B. Chabaud, and B. Hébral, *Ultimate regime of convection: Robustness to poor thermal reservoirs*, Phys. Fluids **17**, 115107 (4 pages) (2005).
- [33] F. Gauthier and P. Roche, *Evidence of a boundary layer instability at very high Rayleigh number*, EPL **83**, 24005 (6 pages) (2008).
- [34] F. Gauthier, J. Salort, O. Bourgeois, J. Garden, R. du Puits, A. Thess, and P. Roche, *Transition on local temperature fluctuations in highly turbulent convection*, EPL **87**, 44006 (6 pages) (2009).
- [35] P.-E. Roche, F. Gauthier, R. Kaiser, and J. Salort, *On the triggering of the Ultimate Regime of convection*, New J. Phys. **12**, 085014 (2010).
- [36] X. He, D. Funfschilling, H. Nobach, E. Bodenschatz, and G. Ahlers, *Transition to the Ultimate State of Turbulent Rayleigh-Bénard Convection*, Phys. Rev. Lett. **108**, 024502 (2012).
- [37] A. Fleischer and R. Goldstein, *High-Rayleigh-number convection of pressurized gases in a horizontal enclosure*, J. Fluid Mech. **469**, 1 (2002).
- [38] J. J. Niemela and K. R. Sreenivasan, *Confined turbulent convection*, J. Fluid Mech. **481**, 355 (2003).
- [39] J. J. Niemela and K. R. Sreenivasan, *Turbulent convection at high Rayleigh numbers and aspect ratio 4*, J. Fluid Mech. **557**, 411 (2006).
- [40] P. Urban, V. Musilová, and L. Skrbek, *Efficiency of Heat Transfer in Turbulent Rayleigh-Bénard Convection*, Phys. Rev. Lett. **107**, 014302 (2011).
- [41] G. Ahlers, D. Funfschilling, and E. Bodenschatz, *Transitions in heat transport by turbulent convection for $Pr = 0.8$ and $10^{11} \leq Ra \leq 10^{15}$* , New J. Phys. **11**, 123001 (2009).
- [42] G. Ahlers, D. Funfschilling, and E. Bodenschatz, *Addendum to Transitions in heat transport by turbulent convection for $Pr = 0.8$ and $10^{11} \leq Ra \leq 10^{15}$* , New J. Phys. **13**, 049401 (2011).
- [43] G. Ahlers, D. Funfschilling, and E. Bodenschatz, *Transitions in heat transport by turbulent convection for $Pr = 0.8$ and $Ra \lesssim 10^{15}$* , J. Phys.: Conf. Ser. **318**, 082001 (2011).
- [44] L. Liu and G. Ahlers, *Rayleigh-Bénard convection in binary gas mixtures: Thermophysical properties and the onset of convection*, Phys. Rev. E **55**, 6950 (1997).
- [45] G. Ahlers, *Effect of sidewall conductance on heat-transport measurements for turbulent Rayleigh-Bénard convection*, Phys. Rev. E **63**, R015303 (2000).
- [46] P. Roche, B. Castaing, B. Chabaud, B. Hebral, and J. Sommeria, *Side wall effects in Rayleigh Bénard experiments*, Eur. Phys. J. **24**, 405 (2001).
- [47] L. Skrbek, private communication, April 2012.
- [48] A. Oberbeck, *Über die Wärmeleitung der Flüssigkeiten bei Berücksichtigung der Strömungen infolge von Temperaturdifferenzen*, Ann. Phys. Chem. **7**, 271 (1879).
- [49] J. Boussinesq, *Theorie analytique de la chaleur, Vol. 2* (Gauthier-Villars, Paris, 1903).
- [50] G. Ahlers, E. Brown, F. Fontenele Araujo, D. Funfschilling, S. Grossmann, and D. Lohse, *Non-Oberbeck-Boussinesq effects in strongly turbulent Rayleigh-Bénard convection*, J. Fluid Mech. **569**, 409 (2006).
- [51] G. Ahlers, F. Fontenele Araujo, D. Funfschilling, S. Grossmann, and D. Lohse, *Non-Oberbeck-Boussinesq effects in gaseous Rayleigh-Bénard convection*, Phys. Rev. Lett. **98**, 054501 (2007).

- [52] G. Ahlers, E. Calzavarini, F. Fontenele Araujo, D. Funfschilling, S. Grossmann, D. Lohse, and K. Sugiyama, *Non-Oberbeck-Boussinesq effects in turbulent thermal convection in ethane close to the critical point*, Phys. Rev. E **77**, 046302 (2008).
- [53] D. Funfschilling, E. Bodenschatz, and G. Ahlers, *Search for the “ultimate state” in turbulent Rayleigh-Bénard convection*, Phys. Rev. Lett. **103**, 014503 (2009).
- [54] J. Niemela and K. Sreenivasan, *Does confined turbulent convection ever attain the “asymptotic scaling” with 1/2-power?*, New J. Phys. **12**, 115002 (2010).
- [55] W. S. O. Shishkina, and C. Wagner, *Boundary layers and wind in cylindrical RayleighBénard cells*, J. Fluid Mech. **697**, 336 (2012).
- [56] S. Grossmann and D. Lohse, *Prandtl and Rayleigh number dependence of the Reynolds number in turbulent thermal convection*, Phys. Rev. E **66**, 016305 (2002).